AN ENERGY AND MOMENTUM CONSERVING SCHEME FOR MORTAR CONTACT METHODS

Christian Hesch[‡] and **Peter Betsch**
Chair of Computational Mechanics
Department of Mechanical Engineering
University of Siegen, 57068 Siegen, Germany

Abstract

We aim at the design of energy-momentum schemes applicable to Mortar-based contact formulation. From the outset we regard the semi-discrete contact problem as finite-dimensional mechanical system subject to (holonomic) contact constraints. Accordingly, the equations of motion assume the form of differential-algebraic equations (DAEs). Energy-momentum schemes emanating from the direct discretization of the DAEs have been recently developed, see Gonzalez [9] and Betsch & Steinmann [6]. In particular, our approach to the design of energy-momentum schemes makes direct use of the invariance properties of the discrete contact constraints by exploring the representation theorem due to Cauchy. Furthermore, special requirements for the algorithmic conservation of energy in the case of high velocity impact are analyzed.

1 Introduction

The present work deals with large deformation contact problems within a nonlinear finite element framework. For a survey of previous developments in this field we refer to the books by Laursen [10] and Wriggers [16]. We restrict our attention to the frictionless dynamic contact of elastic bodies. The corresponding semi-discrete system can be classified as Hamiltonian system with symmetry. Consequently, the momentum maps associated with specific symmetries as well as the total energy are conserved quantities of the underlying finite-dimensional system.

Energy-momentum conserving schemes (and energy decaying variants thereof) have previously been developed in the framework of nonlinear elastodynamics in order to meet the numerical stability requirements of finite-deformation problems, see, for example, Simo & Tarnow [13] and Betsch & Steinmann [5].

Finite deformation contact problems put even higher demands on the numerical stability properties of time-stepping schemes. It is thus not surprising that recently published works aim at the extension of energy-momentum schemes to the realm of contact/impact problems. To this end Laursen & Chawla [11] enforce the discrete gap rate rather than the constraint of impenetrability. Similarly, Armero & Petöcz [3] modify the contact constraint to achieve the desired conservation properties. Consequently, in both works the impenetrability condition is violated in general. Alternatively, Laursen & Love [12] enforce the constraint of impenetrability and achieve algorithmic energy conservation by introducing a so-called discrete contact velocity. However, this approach requires the solution of quadratic equations which turn out to be unsolvable in some events. It is further worth noting that the aforementioned developments have been carried out within the framework of the Mortar formulation of the contact problem.

In the present work we aim at the design of energy-momentum schemes for contact problems in the framework of the Mortar formulation. From the outset we regard the semi-discrete contact problem as finite-dimensional Hamiltonian system subject to (holonomic) contact constraints. Accordingly, the equations of motion assume the form of differential-algebraic equations (DAEs). Energy-momentum schemes emanating from the direct discretization of the DAEs have been recently developed, see Gonzalez [9] and Betsch & Steinmann [6]. Based on these developments our approach to the design of energy-momentum schemes makes use of the invariance properties of the discrete contact constraints by exploring the representation theorem due to Cauchy.

An outline of the rest of the paper is as follows. Section 2 deals with the Hamiltonian formulation of semi-discrete elastodynamics. In this connection, the incorporation of algebraic constraints is treated and the relevant conservation properties are outlined. In Section 3 the energy-momentum conserving discretization of the underlying DAEs is dealt with. In particular, the notion of a discrete gradient is introduced in conjunction with Cauchy's representation theorem. This approach is then particularized to the Mortar description of the contact problem. After the treatment of a representative numerical example in Section 5, conclusions are drawn in Section 6.

[‡]Corresponding author, email: hesch@imr.mb.uni-siegen.de

2 Hamiltonian formulation of semi-discrete elastodynamics

We start with the space finite element discretization of nonlinear elastodynamics. In particular, we aim at the Hamiltonian formulation of the resulting semi-discrete problem. Further details of the present discretization approach may be found in Simo [1, CHAPTER IV] and the works cited therein.

2.1 The free semi-discrete elastic body

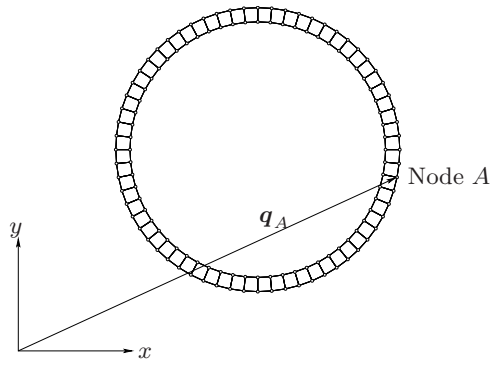

Figure 1: Planar ($n_{dim} = 2$) sketch of a free semi-discrete body.

We first focus on the space discretization of the free elastic body (i.e. pure Neumann boundary conditions). Let $\mathcal{B}$ be a regular region in n_{dim}-dimensional Euclidean space ($n_{dim} \leq 3$) occupied by the reference configuration of the elastic body. Furthermore, let $\mathbb{I} = [0, T]$ denote the time interval of interest. From a kinematic point of view the standard displacement-based finite element approach employs an approximation of the deformation field $\boldsymbol{\varphi} : \mathcal{B} \times \mathbb{I} \to \mathbb{R}^{n_{dim}}$ of the form

$$\boldsymbol{\varphi}(\boldsymbol{X}, t) = \sum_{A=1}^{n_{node}} N_A(\boldsymbol{X}) \boldsymbol{q}_A(t) \tag{1}$$

Within the material (or Lagrangian) description of motion $\boldsymbol{\varphi}(\boldsymbol{X}, t)$ describes the position of material point $\boldsymbol{X}$ of body $\mathcal{B}$ at time t. Moreover, $N_A : \mathcal{B} \to \mathbb{R}$ are global shape functions associated with the nodes $A = 1, ..., n_{node}$ and $\boldsymbol{q}_A : \mathbb{I} \to \mathbb{R}^{n_{dim}}$ denotes the position vector at time $t \in \mathbb{I}$ of the nodal point A (Fig. 1). Accordingly, possible configurations of the semi-discrete dynamical system at hand are characterized by

$$\boldsymbol{q} = (\boldsymbol{q}_1, ..., \boldsymbol{q}_{n_{node}}) \in \mathbb{R}^{n_{dof}} \tag{2}$$

where $n_{dof} = n_{dim} \cdot n_{node}$. The material velocity is defined by $\boldsymbol{v} = \partial\boldsymbol{\varphi}/\partial t = \dot{\boldsymbol{\varphi}}$ such that the finite element approximation implies

$$\boldsymbol{v}(\boldsymbol{X}, t) = \sum_{A=1}^{n_{node}} N_A(\boldsymbol{X}) \boldsymbol{v}_A(t) \tag{3}$$

with $\boldsymbol{v}_A = \dot{\boldsymbol{q}}_A$. Moreover, the finite element approximation (1) gives rise to the discrete deformation gradient

$$\boldsymbol{F} = \frac{\partial \boldsymbol{\varphi}}{\partial \boldsymbol{X}} = \sum_{A=1}^{n_{node}} \boldsymbol{q}_A \otimes \nabla N_A(\boldsymbol{X}) \tag{4}$$

Then the discrete version of the deformation tensor (or right Cauchy-Green tensor) $\boldsymbol{C} = \boldsymbol{F}^T \boldsymbol{F}$ can be written as

$$\boldsymbol{C} = \sum_{A,B=1}^{n_{node}} \boldsymbol{q}_A \cdot \boldsymbol{q}_B \nabla N_A \otimes \nabla N_B \tag{5}$$

Hyperelastic material behavior is modeled by means of a scalar-valued strain energy density function $W(\boldsymbol{C})$ such that the second Piola-Kirchhoff stress tensor can be calculated via

$$\boldsymbol{S} = 2DW(\boldsymbol{C}) \tag{6}$$

where $DW(\boldsymbol{C}) = \partial W/\partial \boldsymbol{C}$. Then the discrete strain energy function is given by

$$V^{int}(\boldsymbol{q}) = \int_{\mathcal{B}} W(\boldsymbol{C}) dV \tag{7}$$

For simplicity we assume that the external forces acting on the body can be derived from a potential function

$$V^{ext} = -\int_{\mathcal{B}} \varrho_R \boldsymbol{b} \cdot \boldsymbol{\varphi}\, dV - \int_{\partial\mathcal{B}_\sigma} \bar{\boldsymbol{t}} \cdot \boldsymbol{\varphi}\, dA \tag{8}$$

where $\varrho_R : \mathcal{B} \to \mathbb{R}_+$ denotes the reference mass density, $\boldsymbol{b} : \mathcal{B} \times \mathbb{I} \to \mathbb{R}^{n_{dim}}$ is the applied body force and $\bar{\boldsymbol{t}}$ is the prescribed traction boundary condition on $\partial\mathcal{B}_\sigma \times \mathbb{I}$. In view of (1) one obtains

$$V^{ext}(\boldsymbol{q}) = -\sum_{A=1}^{n_{node}} \boldsymbol{q}_A \cdot \boldsymbol{F}_A^{ext} \tag{9}$$

with prescribed external nodal forces

$$\boldsymbol{F}_A^{ext} = \int_{\mathcal{B}} N_A \varrho_R \boldsymbol{b}\, dV + \int_{\partial\mathcal{B}_\sigma} N_A \bar{\boldsymbol{t}}\, dA \tag{10}$$

The kinetic energy of the body at time t is given by

$$T = \frac{1}{2} \int_{\mathcal{B}} \varrho_R \boldsymbol{v} \cdot \boldsymbol{v}\, dV \tag{11}$$

such that substitution from (3) into (11) leads to

$$T(\boldsymbol{v}) = \frac{1}{2} \sum_{A,B=1}^{n_{node}} M_{AB} \boldsymbol{v}_A \cdot \boldsymbol{v}_B = \frac{1}{2} \boldsymbol{v} \cdot \boldsymbol{M} \boldsymbol{v} \tag{12}$$

where

$$M_{AB} = \int_{\mathcal{B}} \varrho_R N_A N_B\, dV \tag{13}$$

are the coefficients of the consistent mass matrix. Note that $\boldsymbol{M}$ consists of diagonal sub-matrices $\boldsymbol{M}_{AB} = M_{AB} \boldsymbol{I}_{n_{dim}}$ with $A, B = 1, ..., n_{node}$. The Lagrangian of the finite-dimensional dynamical system under consideration is given by $L(\boldsymbol{q}, \boldsymbol{v}) = T(\boldsymbol{v}) - \big(V^{int}(\boldsymbol{q}) + V^{ext}(\boldsymbol{q})\big)$. To perform the transition to the Hamiltonian formulation we introduce the conjugate momenta

$$\boldsymbol{p} = \frac{\partial L}{\partial \boldsymbol{v}} = \boldsymbol{M} \boldsymbol{v} \tag{14}$$

Then the Hamiltonian function follows from the Legendre transformation of $L(\boldsymbol{q}, \boldsymbol{v})$ with respect to $\boldsymbol{v}$ as $H(\boldsymbol{q}, \boldsymbol{p}) =$

$\boldsymbol{p}\cdot\boldsymbol{v} - L(\boldsymbol{q},\boldsymbol{v})$, with the velocities $\boldsymbol{v}$ being replaced by the momenta in (14). Accordingly, the Hamiltonian of the free semi-discrete elastic body can be written in the form

$$H(\boldsymbol{q},\boldsymbol{p}) = \frac{1}{2}\boldsymbol{p}\cdot\boldsymbol{M}^{-1}\boldsymbol{p} + V^{int}(\boldsymbol{q}) + V^{ext}(\boldsymbol{q}) \tag{15}$$

Consequently, the equations of motion can be written in canonical Hamiltonian form

$$\begin{aligned} \dot{\boldsymbol{q}} &= \frac{\partial H}{\partial \boldsymbol{p}} &&= \boldsymbol{M}^{-1}\boldsymbol{p} \\ \dot{\boldsymbol{p}} &= -\frac{\partial H}{\partial \boldsymbol{q}} &&= \boldsymbol{F}^{ext} - \boldsymbol{F}^{int}(\boldsymbol{q}) \end{aligned} \tag{16}$$

In this connection, the internal forces are given by

$$\boldsymbol{F}^{int}(\boldsymbol{q}) = \nabla V^{int}(\boldsymbol{q}) \tag{17}$$

A more compact description of the equations of motion can be achieved by introducing the vector of phase space coordinates

$$\boldsymbol{z} = (\boldsymbol{q},\boldsymbol{p}) \in \mathbb{R}^{2n_{dof}} \tag{18}$$

Then the equations of motion pertaining to the semi-discrete free elastic body can alternatively be written as

$$\dot{\boldsymbol{z}} = \mathbb{J}\nabla H(\boldsymbol{z}) \tag{19}$$

In the last equation $\mathbb{J} \in \mathbb{R}^{2n_{dof}\times 2n_{dof}}$ is the canonical symplectic matrix

$$\mathbb{J} = \begin{bmatrix} \boldsymbol{0} & \boldsymbol{I} \\ -\boldsymbol{I} & \boldsymbol{0} \end{bmatrix} \tag{20}$$

where $\boldsymbol{I}$ and $\boldsymbol{0}$ are the $n_{dof}\times n_{dof}$ identity and zero matrices. Note that $\mathbb{J}^T = \mathbb{J}^{-1} = -\mathbb{J}$ and $\mathbb{J}^2 = -\mathbb{I}$, where $\mathbb{I}$ denotes the $(2n_{dof}\times 2n_{dof})$ identity matrix.

2.2 Constrained semi-discrete elastic bodies

We next focus on specific boundary conditions which restrict the motion of the semi-discrete elastic body. These restrictions can be characterized by geometric constraints acting on the boundary nodes of the discrete system at hand. In particular, we distinguish between Dirichlet-type boundary conditions and constraints due to contact. For the present purposes it suffices to consider the planar two-body contact problem (Fig. 2).

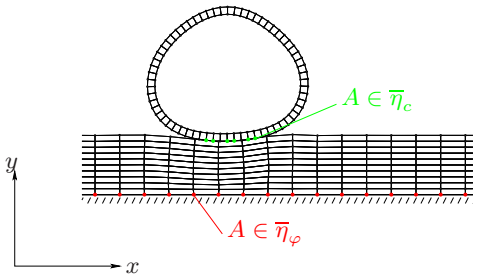

Figure 2: The planar two-body contact problem.

Assume that n_{node} denotes the total number of nodes due to the space discretization of the two elastic bodies, so that $\eta = \{1,\dots,n_{node}\}$ is the set of node numbers associated with the discrete two-body system. Further let $\overline{\eta} \subset \eta$ be the set of node numbers lying on the boundaries of the two-body system. The relevant boundary conditions can be characterized by algebraic constraints of the form

$$\boldsymbol{\Phi}(\boldsymbol{q}) = \boldsymbol{0} \tag{21}$$

In the case of Dirichlet-type boundary conditions we have

$$\boldsymbol{q}_A(t) = \overline{\boldsymbol{\varphi}}(\boldsymbol{X}_A, t)\,, \quad \text{for } A \in \overline{\eta}_\varphi \tag{22}$$

where $\overline{\boldsymbol{\varphi}}_t$ is prescribed and $\overline{\eta}_\varphi \subset \overline{\eta}$ is the set of node numbers belonging to the Dirichlet boundary. Similarly, if the two bodies are in contact and provided that 'active' nodes $A \in \overline{\eta}_c \subset \overline{\eta} - \overline{\eta}_\varphi$ lying on the contact surface have been detected, additional constraints of the form (21) arise (see Section 4 for further details). Due to the presence of the constraints (21), the equations of motion can now be written in the form

$$\begin{aligned} \dot{\boldsymbol{q}} &= \frac{\partial H}{\partial \boldsymbol{p}} \\ \dot{\boldsymbol{p}} &= -\frac{\partial H}{\partial \boldsymbol{q}} - D\boldsymbol{\Phi}(\boldsymbol{q})^T\boldsymbol{\lambda} \\ \boldsymbol{0} &= \boldsymbol{\Phi}(\boldsymbol{q}) \end{aligned} \tag{23}$$

where $\boldsymbol{\Phi}(\boldsymbol{q}) \in \mathbb{R}^m$ are the relevant constraint functions, $D\boldsymbol{\Phi}(\boldsymbol{q})$ is the corresponding constraint Jacobian and $\boldsymbol{\lambda} \in \mathbb{R}^m$ are Lagrange multipliers which determine the size of the constraint forces in $(23)_2$. Similar to (19), the set of differential-algebraic equations (DAEs) in (23) can be rewritten in compact form by introducing the augmented Hamiltonian

$$\mathcal{H}_\lambda(\boldsymbol{z}) = \frac{1}{2}\boldsymbol{p}\cdot\boldsymbol{M}^{-1}\boldsymbol{p} + \mathcal{V}_\lambda(\boldsymbol{q}) \tag{24}$$

where

$$\mathcal{V}_\lambda(\boldsymbol{q}) = V^{int}(\boldsymbol{q}) + V^{ext}(\boldsymbol{q}) + \boldsymbol{\lambda}\cdot\boldsymbol{\Phi}(\boldsymbol{q}) \tag{25}$$

is an augmented potential function. Now the differential part of the DAEs can be written as

$$\dot{\boldsymbol{z}} = \mathbb{J}\nabla\mathcal{H}_\lambda(\boldsymbol{z}) \tag{26}$$

which, of course, has to be supplemented with the algebraic constraints $(23)_3$.

3 Energy-momentum scheme

We next outline the design of a time-stepping scheme which is able to reproduce for any step-size the crucial conservation properties summarized above. Concerning the time discretization of the DAEs (23), we apply the Galerkin-based approach developed by Betsch & Steinmann [5]. To this end, we consider a characteristic time-step $\Delta t = t_{n+1} - t_n$ and restrict our attention to linear approximations (the so-called mG(1) method in [5]) of the form

$$\boldsymbol{z}^h(\alpha) = (1-\alpha)\boldsymbol{z}_n + \alpha\boldsymbol{z}_{n+1} \quad \text{for} \quad \alpha \in [0,1] \tag{27}$$

In this connection all quantities at t_n, such as $\boldsymbol{z}_n$, can be regarded as being given. Note that (27) leads to a globally continuous approximation of the phase space coordinates. In

contrast to that, the Lagrange multipliers are assumed to be piecewise constant in each time-step, i.e.

$$\boldsymbol{\lambda}^h = \boldsymbol{\lambda}_{n+1} \tag{28}$$

The mG(1) method yields

$$\boldsymbol{z}_{n+1} - \boldsymbol{z}_n = \Delta t \mathbb{J} \int_0^1 \nabla \mathcal{H}_{\lambda^h}(\boldsymbol{z}^h)\, d\alpha \tag{29}$$

It is shown in [5] that the application of a specific quadrature formula for the evaluation of the time integral in (29) has a strong impact on the conservation properties of the resulting time-stepping scheme. In the present work we choose

$$\int_0^1 \nabla \mathcal{H}_{\lambda^h}(\boldsymbol{z}^h)\, d\alpha \approx \bar{\nabla} \mathcal{H}_{\lambda_{n+1}}(\boldsymbol{z}_n, \boldsymbol{z}_{n+1}) \tag{30}$$

where $\bar{\nabla}\mathcal{H}_\lambda(z_n, z_{n+1})$ is a discrete gradient (or derivative) in the sense of Gonzalez [8]. It is shown in [8] that the discrete gradient can be designed such that the desired conservation properties are satisfied and specific consistency and accuracy requirements are met. To achieve this goal we aim at a reparametrization of the augmented Hamiltonian which incorporates the invariance properties in a natural way. For example, assume that the rotational invariance property holds and that the augmented Hamiltonian depends only on $\mathbb{S}(\boldsymbol{z})$, where

$$\begin{aligned}\mathbb{S}(\boldsymbol{z}) &= \mathbb{S}(\boldsymbol{z}_1, \ldots, \boldsymbol{z}_N) \\ &= \{\boldsymbol{y}_A \cdot \boldsymbol{y}_B\,, 1 \le A \le B \le n_{node}\,, \boldsymbol{y}_A \in \{\boldsymbol{q}_A, \boldsymbol{p}_A\}\}\end{aligned} \tag{31}$$

is the set of (quadratic) invariants of $\boldsymbol{z} \in \mathbb{R}^{2n_{dof}}$. It is worth mentioning that this approach is in accordance with Cauchy's Representation Theorem (see, for example, Truesdell & Noll [15, Sect. 11.]). Accordingly, the augmented Hamiltonian can now be written in the form

$$\mathcal{H}_\lambda(\boldsymbol{z}) = \widetilde{\mathcal{H}}_\lambda\left(\boldsymbol{\pi}(\boldsymbol{z})\right) \tag{32}$$

where the vector of relevant invariants

$$\boldsymbol{\pi}(\boldsymbol{z}) = \begin{bmatrix} \pi_1(\boldsymbol{z}) \\ \vdots \\ \pi_d(\boldsymbol{z}) \end{bmatrix} \tag{33}$$

has been introduced. Note that the components $\pi_i(\boldsymbol{z})$ depend only on $\mathbb{S}(\boldsymbol{z})$. In the following we make use of Gonzalez' [8] definition of the discrete gradient. Accordingly, in the present context, the discrete gradient of the augmented Hamiltonian assumes the form

$$\boxed{\bar{\nabla}\mathcal{H}_\lambda(\boldsymbol{z}_n, \boldsymbol{z}_{n+1}) = D\boldsymbol{\pi}(\boldsymbol{z}_{n+\frac{1}{2}})^T \bar{\bar{\nabla}}\widetilde{\mathcal{H}}_\lambda\big(\boldsymbol{\pi}(\boldsymbol{z}_n), \boldsymbol{\pi}(\boldsymbol{z}_{n+1})\big)} \tag{34}$$

with

$$\begin{aligned}\bar{\bar{\nabla}}\widetilde{\mathcal{H}}_\lambda\big(\boldsymbol{\pi}_n, \boldsymbol{\pi}_{n+1}\big) &= \nabla\widetilde{\mathcal{H}}_\lambda(\boldsymbol{\pi}_{n+\frac{1}{2}}) + \\ &\frac{\widetilde{\mathcal{H}}_\lambda(\boldsymbol{\pi}_{n+1}) - \widetilde{\mathcal{H}}_\lambda(\boldsymbol{\pi}_n) - \nabla\widetilde{\mathcal{H}}_\lambda(\boldsymbol{\pi}_{n+\frac{1}{2}}) \cdot (\boldsymbol{\pi}_{n+1} - \boldsymbol{\pi}_n)}{\| \boldsymbol{\pi}_{n+1} - \boldsymbol{\pi}_n \|^2} \times \\ &(\boldsymbol{\pi}_{n+1} - \boldsymbol{\pi}_n)\end{aligned} \tag{35}$$

and

$$\begin{aligned}\boldsymbol{z}_{n+\frac{1}{2}} &= \frac{1}{2}(\boldsymbol{z}_n + \boldsymbol{z}_{n+1}) \\ \boldsymbol{\pi}_{n+\frac{1}{2}} &= \frac{1}{2}(\boldsymbol{\pi}_n + \boldsymbol{\pi}_{n+1})\end{aligned} \tag{36}$$

To summarize, the mG(1) method with quadrature formula (30) yields the following time-stepping scheme:

$$\begin{aligned}\boldsymbol{z}_{n+1} &= \boldsymbol{z}_n + \Delta t \mathbb{J} \bar{\nabla}\mathcal{H}_{\lambda_{n+1}}(\boldsymbol{z}_n, \boldsymbol{z}_{n+1}) \\ \boldsymbol{0} &= \boldsymbol{\Phi}(\boldsymbol{q}_{n+1})\end{aligned} \tag{37}$$

In essence, the scheme (37) is equivalent to the method proposed by Gonzalez [9]. We further remark that in addition to the constraints on configuration level $(37)_2$, the constraints on momentum level, i.e. $d\boldsymbol{\Phi}(\boldsymbol{q})/dt = D\boldsymbol{\Phi}(\boldsymbol{q})\boldsymbol{M}^{-1}\boldsymbol{p} = \boldsymbol{0}$ can be enforced at the end of the time step by adjusting the GGL-type [7] technique to the present conserving framework, see [5] for further details. However, numerical tests revealed no significant improvement of the numerical performance which would justify the additional computational effort.
If a function $f(\boldsymbol{z})$ is merely quadratic it may be written as $f(\boldsymbol{z}) = \widetilde{f}\big(\boldsymbol{\pi}(\boldsymbol{z})\big) = \boldsymbol{a} \cdot \boldsymbol{\pi}(\boldsymbol{z})$, with constant $\boldsymbol{a} \in \mathbb{R}^d$. It can be easily verified that the corresponding discrete gradient is given by

$$\bar{\nabla} f(\boldsymbol{z}_n, \boldsymbol{z}_{n+1}) = D\boldsymbol{\pi}(\boldsymbol{z}_{n+\frac{1}{2}})^T \boldsymbol{a} = \nabla f(\boldsymbol{z}_{n+\frac{1}{2}}) \tag{38}$$

Accordingly, in this case the discrete gradient coincides with the standard gradient evaluated in $\boldsymbol{z}_{n+\frac{1}{2}}$.

3.1 Algorithmic conservation properties

Similar to the continuous case dealt with before, we next verify that the scheme (37) indeed satisfies the relevant conservation laws.

3.1.1 Algorithmic conservation of the total angular momentum

The fundamental theorem of calculus gives

$$\begin{aligned}J_\xi(\boldsymbol{z}_{n+1}) - J_\xi(\boldsymbol{z}_n) &= \int_0^1 \nabla J_\xi\left(\boldsymbol{z}^h(\alpha)\right) \cdot \left(\boldsymbol{z}^h(\alpha)\right)' \,\mathrm{d}\,\alpha \\ &= \int_0^1 \boldsymbol{\xi}_P\left(\boldsymbol{z}^h(\alpha)\right) \,\mathrm{d}\,\alpha \cdot \mathbb{J}(\boldsymbol{z}_{n+1} - \boldsymbol{z}_n) \\ &= \boldsymbol{\xi}_P\left(\boldsymbol{z}_{n+\frac{1}{2}}\right) \cdot \mathbb{J}(\boldsymbol{z}_{n+1} - \boldsymbol{z}_n) \\ &= \boldsymbol{\xi}_P\left(\boldsymbol{z}_{n+\frac{1}{2}}\right) \cdot \mathbb{J}^2 \Delta t \bar{\nabla}\mathcal{H}_{\lambda_{n+1}}(\boldsymbol{z}_n, \boldsymbol{z}_{n+1}) \\ &= -\Delta t \bar{\nabla}\mathcal{H}_{\lambda_{n+1}}(\boldsymbol{z}_n, \boldsymbol{z}_{n+1}) \cdot \boldsymbol{\xi}_P\big(\boldsymbol{z}_{n+\frac{1}{2}}\big) \\ &= -\Delta t \bar{\bar{\nabla}}\widetilde{\mathcal{H}}_{\lambda_{n+1}}\left(\boldsymbol{\pi}(\boldsymbol{z}_n), \boldsymbol{\pi}(\boldsymbol{z}_{n+1})\right) \cdot D\boldsymbol{\pi}(\boldsymbol{z}_{n+\frac{1}{2}}) \boldsymbol{\xi}_P\left(\boldsymbol{z}_{n+\frac{1}{2}}\right) \\ &= 0\end{aligned} \tag{39}$$

where use has been made of the property

$$\boldsymbol{0} = \left.\frac{d}{d\varepsilon}\right|_{\varepsilon=0} \boldsymbol{\pi}(\exp(\varepsilon\hat{\boldsymbol{\xi}}) \circ \boldsymbol{z}) = D\boldsymbol{\pi}(\boldsymbol{z})\boldsymbol{\xi}_P(\boldsymbol{z}) \tag{40}$$

which holds due to the rotational invariance of the vector-valued function $\boldsymbol{\pi}(\boldsymbol{z})$. Equation (39) corroborates algorithmic conservation of the total angular momentum.

3.1.2 Algorithmic conservation of the total energy

In the discrete setting we get

$$\frac{1}{\Delta t}\bar{\nabla}\mathcal{H}_{\lambda_{n+1}}(\boldsymbol{z}_n,\boldsymbol{z}_{n+1})\cdot(\boldsymbol{z}_{n+1}-\boldsymbol{z}_n)=\bar{\nabla}\mathcal{H}_{\lambda_{n+1}}\cdot\mathbb{J}\bar{\nabla}\mathcal{H}_{\lambda_{n+1}}=0 \tag{41}$$

On the other hand, with regard to the discrete gradient (34), we obtain

$$\begin{aligned}
&\bar{\nabla}\mathcal{H}_{\lambda_{n+1}}(\boldsymbol{z}_n,\boldsymbol{z}_{n+1})\cdot(\boldsymbol{z}_{n+1}-\boldsymbol{z}_n)\\
&\quad=\bar{\bar{\nabla}}\widetilde{\mathcal{H}}_{\lambda_{n+1}}\left(\boldsymbol{\pi}(\boldsymbol{z}_n),\boldsymbol{\pi}(\boldsymbol{z}_{n+1})\right)\cdot D\boldsymbol{\pi}(\boldsymbol{z}_{n+\frac{1}{2}})\cdot(\boldsymbol{z}_{n+1}-\boldsymbol{z}_n)\\
&\quad=\bar{\bar{\nabla}}\widetilde{\mathcal{H}}_{\lambda_{n+1}}\left(\boldsymbol{\pi}(\boldsymbol{z}_n),\boldsymbol{\pi}(\boldsymbol{z}_{n+1})\right)\cdot(\boldsymbol{\pi}(\boldsymbol{z}_{n+1})-\boldsymbol{\pi}(\boldsymbol{z}_n))\\
&\quad=\widetilde{\mathcal{H}}_{\lambda_{n+1}}\left(\boldsymbol{\pi}(\boldsymbol{z}_{n+1})\right)-\widetilde{\mathcal{H}}_{\lambda_{n+1}}\left(\boldsymbol{\pi}(\boldsymbol{z}_n)\right)\\
&\quad=\mathcal{H}_{\lambda_{n+1}}(\boldsymbol{z}_{n+1})-\mathcal{H}_{\lambda_{n+1}}(\boldsymbol{z}_n)\\
&\quad=H(\boldsymbol{z}_{n+1})-H(\boldsymbol{z}_n)+\boldsymbol{\lambda}_{n+1}\cdot\left(\boldsymbol{\Phi}(\boldsymbol{q}_{n+1})-\boldsymbol{\Phi}(\boldsymbol{q}_n)\right)\\
&\quad=H(\boldsymbol{z}_{n+1})-H(\boldsymbol{z}_n)
\end{aligned} \tag{42}$$

where use has been made of (35) and (37) and the fact that the invariants $\boldsymbol{\pi}(\boldsymbol{z})$ are quadratic functions. Comparison of (41) and (42) yields

$$H(\boldsymbol{z}_{n+1})=H(\boldsymbol{z}_n) \tag{43}$$

which confirms algorithmic conservation of the total energy.

3.2 Final form of the energy-momentum scheme

We next exploit the specific (separable) form of the augmented Hamiltonian (24) to recast the energy-momentum scheme (37) in an alternative form which is especially well-suited for the computer implementation. With regard to (12), the kinetic energy in (24) can be written as

$$T(\boldsymbol{p})=\frac{1}{2}\sum_{A,B=1}^{n_{node}}M^{-1}_{AB}\boldsymbol{p}_A\cdot\boldsymbol{p}_B \tag{44}$$

and is thus merely a quadratic function of the nodal momenta. In this connection, the inverse of the mass matrix is composed of diagonal sub-matrices $\boldsymbol{M}^{-1}_{AB}=M^{-1}_{AB}\boldsymbol{I}_{n_{dim}}$ $(A,B=1,\ldots,n_{node})$. Taking into account Remark 3, the discrete gradient of the augmented Hamiltonian (34) can be written in simplified form

$$\bar{\nabla}\mathcal{H}_\lambda(\boldsymbol{z}_n,\boldsymbol{z}_{n+1})=\begin{bmatrix}\bar{\nabla}_q\mathcal{V}_\lambda(\boldsymbol{q}_n,\boldsymbol{q}_{n+1})\\ \bar{\nabla}_p T(\boldsymbol{p}_n,\boldsymbol{p}_{n+1})\end{bmatrix}=\begin{bmatrix}\bar{\nabla}_q\mathcal{V}_\lambda(\boldsymbol{q}_n,\boldsymbol{q}_{n+1})\\ \boldsymbol{M}^{-1}\boldsymbol{p}_{n+\frac{1}{2}}\end{bmatrix} \tag{45}$$

Accordingly, application of the discrete gradient is confined to the augmented potential function (25). That is, (34) boils down to

$$\boxed{\bar{\nabla}_q\mathcal{V}_\lambda(\boldsymbol{q}_n,\boldsymbol{q}_{n+1})=D\boldsymbol{\pi}(\boldsymbol{q}_{n+\frac{1}{2}})^T\bar{\bar{\nabla}}\widetilde{\mathcal{V}}_\lambda\left(\boldsymbol{\pi}(\boldsymbol{q}_n),\boldsymbol{\pi}(\boldsymbol{q}_{n+1})\right)} \tag{46}$$

Now the energy-momentum scheme (37) gives rise to the following algorithmic problem:

$$\begin{aligned}
\boldsymbol{q}_{n+1}-\boldsymbol{q}_n&=\frac{\Delta t}{2}\left(\boldsymbol{v}_n+\boldsymbol{v}_{n+1}\right)\\
\boldsymbol{M}(\boldsymbol{v}_{n+1}-\boldsymbol{v}_n)&=-\Delta t\bar{\nabla}_q V(\boldsymbol{q}_n,\boldsymbol{q}_{n+1})\\
&\quad-\Delta t\sum_{l=1}^{m}\left(\lambda_l\right)_{n+1}\bar{\nabla}_q\Phi_l(\boldsymbol{q}_n,\boldsymbol{q}_{n+1})\\
\boldsymbol{0}&=\boldsymbol{\Phi}(\boldsymbol{q}_{n+1})
\end{aligned} \tag{47}$$

3.3 Application to planar problems

The application of the scheme (47) essentially depends on specific parametrizations of the discrete strain energy function $V^{int}(\boldsymbol{q})$ and the constraint functions $\Phi_l(\boldsymbol{q})$ in terms of appropriate invariants. We shall illustrate this procedure by considering planar problems, i.e. $n_{dim}=2$ and $\boldsymbol{q}_A\in\mathbb{R}^2$ $(A\in\eta)$.

As before, we focus on the case of rotational invariance. If a scalar-valued function $\gamma(\boldsymbol{q}_1,\ldots,\boldsymbol{q}_{n_{node}})$ is invariant under the proper orthogonal group, then Cauchy's representation theorem (Truesdell & Noll [15, Sect. 11.] or Antman [2, Chapter 8]) implies that $\gamma(\boldsymbol{q})$ depends only on the set of quadratic invariants $\mathbb{I}(\boldsymbol{q})=\mathbb{S}(\boldsymbol{q})\bigcup\mathbb{T}(\boldsymbol{q})$, where

$$\begin{aligned}
\mathbb{S}(\boldsymbol{q})&=\left\{\boldsymbol{q}_A\cdot\boldsymbol{q}_B\,,1\le A\le B\le n_{nodes}\right\}\\
\mathbb{T}(\boldsymbol{q})&=\left\{\det([\boldsymbol{q}_A,\boldsymbol{q}_B])\,,1\le A<B\le n_{nodes}\right\}
\end{aligned} \tag{48}$$

We first deal with the discrete strain energy function. Thereafter, we focus on the constraint functions corresponding to a specific contact formulation.

4 Mortar method

The basic concept of the mortar method is an integral formulation of the constrain energy, stored in the actual contact surface γ_c

$$\mathcal{V}_\lambda(\boldsymbol{q})=V^{int}(\boldsymbol{q})+V^{ext}(\boldsymbol{q})+\int_{\gamma_c}\boldsymbol{\lambda}^h\cdot(\boldsymbol{x}^{(1)^h}-\boldsymbol{x}^{(2)^h})\,\mathrm{d}\gamma \tag{49}$$

The contact surface is split into segments as shown in figure 3 corresponding to the segment definition proposed by Simo et al. [14]. The Mortar segment is bounded by the four element coordinates $\xi_a^{(1)}$, $\xi_b^{(1)}$, $\xi_a^{(2)}$ and $\xi_b^{(2)}$. A linear mapping $\eta\rightarrow\xi^(i)$ for each segment is given by

$$\xi^{(i)}=\frac{1}{2}(1-\eta)\xi_a^{(i)}+\frac{1}{2}(1+\eta)\xi_b^{(i)} \tag{50}$$

Using this mapping, the Lagrange multipliers and the geometry can be discretised with standard shape functions conform to the underlying geometrie of both bodies in contact, depending on a single parametrisation η

$$\begin{aligned}
\boldsymbol{\lambda}^h&=\sum_A N_A(\xi^{(1)}(\eta))\boldsymbol{\lambda}_A\\
\boldsymbol{x}^{(1)^h}&=\sum_B N_B(\xi^{(1)}(\eta))\boldsymbol{x}_B^{(1)}\\
\boldsymbol{x}^{(2)^h}&=\sum_C N_C(\xi^{(2)}(\eta))\boldsymbol{x}_C^{(2)}
\end{aligned} \tag{51}$$

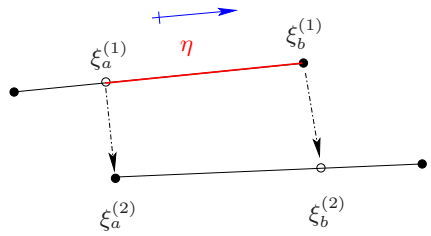

Figure 3: Example for a Mortar segment

where $\boldsymbol{\lambda}_A$ can be decomposed into a normal and a tangential part

$$\boldsymbol{\lambda}_A = \boldsymbol{\lambda}_{N_A} + \boldsymbol{\lambda}_{T_A}; \quad \boldsymbol{\lambda}_{N_A} = \lambda_{N_A} \boldsymbol{n}_A \quad \text{(no sum)} \tag{52}$$

with the normal vector $\boldsymbol{n}_A$. For the constraint of the Mortar method at node A in normal direction follows

$$\Phi_A = \bigcup_{seg} \boldsymbol{n} \cdot \left[n_{AB}^{(1)} \boldsymbol{x}_B^{(1)} - n_{AC}^{(2)} \boldsymbol{x}_C^{(2)} \right] \tag{53}$$

with the Mortar integrals evaluated by a Gauss integration

$$\begin{aligned} n_{AB}^{(1)} &= \int_{\gamma_c^{seg}} N_A^{(1)}(\xi^{(1)}(\eta)) N_B^{(1)}(\xi^{(1)}(\eta)) \, d\gamma \\ &= \sum_{gp} N_A^{(1)}(\xi^{(1)}(\eta_{gp})) N_B^{(1)}(\xi^{(1)}(\eta_{gp})) J_{seg} w_{gp} \end{aligned} \tag{54}$$

and

$$\begin{aligned} n_{AC}^{(2)} &= \int_{\gamma_c^{seg}} N_A^{(1)}(\xi^{(1)}(\eta)) N_C^{(2)}(\xi^{(2)}(\eta)) \, d\gamma \\ &= \sum_{gp} N_A^{(1)}(\xi^{(1)}(\eta_{gp})) N_C^{(2)}(\xi^{(2)}(\eta_{gp})) J_{seg} w_{gp} \end{aligned} \tag{55}$$

with the Gauss weight w_{gp} and the Jacobian at the quadrature point J_{seg}. For the reparametrization of the Mortar constraint with invariants, i.e.

$$\Phi(\boldsymbol{q}) = \widetilde{\Phi}(\boldsymbol{\pi}(\boldsymbol{q})) \tag{56}$$

the first step is to reparametrize the linear mapping, defined in equation (50). Therefor it must be distinguished between a projection onto a node (filled circles in figure 3) and onto a segment (hollow circles in figure 3) respectively. For the projection onto a node follows

$$\xi_1^{(1)} = -1; \quad \xi_2^{(1)} = 1; \quad \xi_1^{(2)} = -1; \quad \xi_2^{(2)} = 1 \tag{57}$$

and for the projection onto a segment

$$\xi_1^{(1)} = \frac{2}{l^2} (\boldsymbol{x}_2^{(1)} - \boldsymbol{x}_1^{(1)}) \cdot (\boldsymbol{x}_1^{(2)} - \boldsymbol{x}_1^{(1)}) - 1 \tag{58}$$

$$\xi_2^{(1)} = \frac{2}{l^2} (\boldsymbol{x}_2^{(1)} - \boldsymbol{x}_1^{(1)}) \cdot (\boldsymbol{x}_2^{(2)} - \boldsymbol{x}_1^{(1)}) - 1 \tag{59}$$

$$\xi_1^{(2)} = \frac{(2\boldsymbol{x}_1^{(1)} - \boldsymbol{x}_1^{(2)} - \boldsymbol{x}_2^{(2)}) \cdot (\boldsymbol{x}_2^{(1)} - \boldsymbol{x}_1^{(1)})}{(\boldsymbol{x}_2^{(2)} - \boldsymbol{x}_1^{(2)}) \cdot (\boldsymbol{x}_2^{(1)} - \boldsymbol{x}_1^{(1)})} \tag{60}$$

$$\xi_2^{(2)} = \frac{(2\boldsymbol{x}_2^{(1)} - \boldsymbol{x}_1^{(2)} - \boldsymbol{x}_2^{(2)}) \cdot (\boldsymbol{x}_2^{(1)} - \boldsymbol{x}_1^{(1)})}{(\boldsymbol{x}_2^{(2)} - \boldsymbol{x}_1^{(2)}) \cdot (\boldsymbol{x}_2^{(1)} - \boldsymbol{x}_1^{(1)})} \tag{61}$$

with

$$l^2 = \boldsymbol{a} \cdot \boldsymbol{a} = (\boldsymbol{x}_2^{(1)} - \boldsymbol{x}_1^{(1)}) \cdot (\boldsymbol{x}_2^{(1)} - \boldsymbol{x}_1^{(1)}) \tag{62}$$

By use of the three invariants

$$\begin{aligned} \pi_1 &= \boldsymbol{a} \cdot \boldsymbol{a} \\ \pi_2 &= \boldsymbol{a} \cdot (\boldsymbol{x}_1^{(2)} - \boldsymbol{x}_1^{(1)}) \\ \pi_3 &= \boldsymbol{a} \cdot (\boldsymbol{x}_2^{(2)} - \boldsymbol{x}_1^{(1)}) \end{aligned} \tag{63}$$

the reparametrization of equation (50) yield

$$\xi^{(1)}(\eta) = \frac{1}{2}(1-\eta) \left[\frac{2}{\pi_1} \pi_2 - 1 \right] + \frac{1}{2}(1+\eta) \left[\frac{2}{\pi_1} \pi_3 - 1 \right] \tag{64}$$

$$\xi^{(2)}(\eta) = \frac{1}{2}(1-\eta) \left[\frac{-\pi_3 - \pi_2}{\pi_3 - \pi_2} \right] + \frac{1}{2}(1+\eta) \left[\frac{2\pi_1 - \pi_3 - \pi_2}{\pi_3 - \pi_2} \right] \tag{65}$$

Applying linear shape functions to $(51)_1$, $(51)_2$ and $(51)_3$ and evaluating the constraint (53) at the Gauss points gp, for each segment follows

$$\begin{aligned} \Phi_{A=1}^{seg,gp} =& \boldsymbol{a} \cdot \boldsymbol{\Lambda} \Bigg\{ \left[\frac{1}{2}(1 - \xi^{(1)}(\eta_{gp})) \frac{1}{2}(1 - \xi^{(1)}(\eta_{gp})) \boldsymbol{x}_1^{(1)} + \right. \\ & \left. \frac{1}{2}(1 - \xi^{(1)}(\eta_{gp})) \frac{1}{2}(1 + \xi^{(1)}(\eta_{gp})) \boldsymbol{x}_2^{(1)} \right] - \\ & \left[\frac{1}{2}(1 - \xi^{(1)}(\eta_{gp})) \frac{1}{2}(1 - \xi^{(2)}(\eta_{gp})) \boldsymbol{x}_1^{(2)} + \right. \\ & \left. \frac{1}{2}(1 - \xi^{(1)}(\eta_{gp})) \frac{1}{2}(1 + \xi^{(2)}(\eta_{gp})) \boldsymbol{x}_2^{(2)} \right] \Bigg\} \times \\ & [\xi_2^{(1)} - \xi_1^{(1)}] w_{gp} / 4 \end{aligned} \tag{66}$$

$$\begin{aligned} =& \boldsymbol{a} \cdot \boldsymbol{\Lambda} [\xi_2^{(1)} - \xi_1^{(1)}] / 16 \Bigg\{ \left[\boldsymbol{x}_1^{(1)} + \boldsymbol{x}_2^{(1)} - \boldsymbol{x}_1^{(2)} - \boldsymbol{x}_2^{(2)} \right] + \\ & \left[\xi^{(1)}(\eta_{gp})(-2\boldsymbol{x}_1^{(1)} + \boldsymbol{x}_1^{(2)} + \boldsymbol{x}_2^{(2)}) + \xi^{(2)}(\eta_{gp})(\boldsymbol{x}_1^{(2)} - \boldsymbol{x}_2^{(2)}) \right] \\ & + \left[\xi^{(1)}(\eta_{gp}) \xi^{(2)}(\eta_{gp})(-\boldsymbol{x}_1^{(2)} + \boldsymbol{x}_2^{(2)}) \right] \Bigg\} w_{gp} \end{aligned} \tag{67}$$

with the constant matrix

$$\boldsymbol{\Lambda} = \begin{bmatrix} 0 & 1 \\ -1 & 0 \end{bmatrix} \tag{68}$$

Two additional invariants are necessary

$$\pi_4 = \boldsymbol{a} \cdot \boldsymbol{\Lambda} (-2\boldsymbol{x}_1^{(1)} + \boldsymbol{x}_1^{(2)} + \boldsymbol{x}_2^{(2)}) \tag{69}$$

$$\pi_5 = \boldsymbol{a} \cdot \boldsymbol{\Lambda} (\boldsymbol{x}_1^{(2)} - \boldsymbol{x}_2^{(2)}) \tag{70}$$

which complets the reparametrization of the Mortar constraint

$$\begin{aligned} \Phi_{A=1}^{seg,gp} = & \frac{1}{16} \left[\left[\frac{2}{\pi_1} \pi_3 - 1 \right] - \left[\frac{2}{\pi_1} \pi_2 - 1 \right] \right] \times \\ & \left\{ (1 - \xi^{(1)}(\eta_{gp})) \pi_4 + (\xi^{(1)}(\eta_{gp}) - \xi^{(1)}(\eta_{gp}) \xi^{(2)}(\eta_{gp})) \pi_5 \right\} \end{aligned} \tag{71}$$

and for $A = 2$ follows

$$\begin{aligned} \Phi_{A=2}^{seg,gp} = & \frac{1}{16} \left[\left[\frac{2}{\pi_1} \pi_3 - 1 \right] - \left[\frac{2}{\pi_1} \pi_2 - 1 \right] \right] \times \\ & \left\{ (1 + \xi^{(1)}(\eta_{gp})) \pi_4 + (\xi^{(1)}(\eta_{gp}) + \xi^{(1)}(\eta_{gp}) \xi^{(2)}(\eta_{gp})) \pi_5 \right\} \end{aligned} \tag{72}$$

The invariants π_1, π_2 and π_3 depends only on $\mathbb{S}$, whereas the invariants π_4 and π_5 depends only on $\mathbb{T}$.

5 Numerical example

5.1 Persistent contact

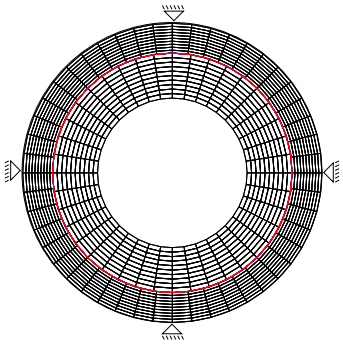

Figure 4: Discretized bearing

The numerical example consists of the planar model of a bearing depicted in Fig. 4, analogue to an example presented in Belytschko et al. [4]. The bearing consists of two rings (Youngs's modulus $E = 10^5$, Poissons's ratio $\nu = 0.1$ and mass density $\varrho_R = 0.001$), which are discretized by 4-node isoparametric displacement-based plain strain elements. The discretization of the outer ring relies on 10x48 elements, for the inner ring 10x40 have been used. The motion of the inner ring is restricted by the condition of persistent contact with the outer ring. Pure Dirichlet-type conditions are applied to fix the outer boundary of the outer ring. To get a pre-stressed initial configuration of the whole bearing, a static equilibrium problem is solved first. To this end the initial outer diameter of the inner ring* ($d_i = 80.1$) exceeds the initial inner diameter of the outer ring† $d_o = 80.0$. Accordingly, the static equilibrium problem consists of enforcing (frictionless) contact between inner and outer ring. The static equilibrium problem is solved in one load increment.

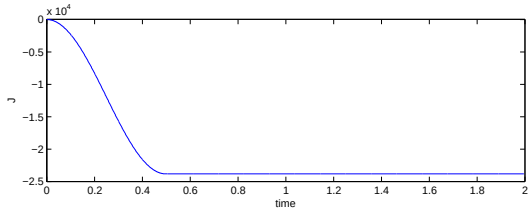

Figure 5: Total angular momentum versus time

After the solution of the equilibrium problem the transient calculation proceeds with $\Delta t = 0.01$. For $t \in [0, 0.5]$, a torque acts on the inner ring in form of a hat function over time. Then, for $t \in (0.5, 2]$, no external loads are acting on the bearing anymore. Fig. 6 shows that for $t \geq 0.5$ the present scheme does indeed conserve the total energy for the frictionless contact problem under consideration. In addition to that, Fig. 5 corroborates algorithmic conservation of angular momentum.

*the inner diameter is 50

†the outer diameter is 100

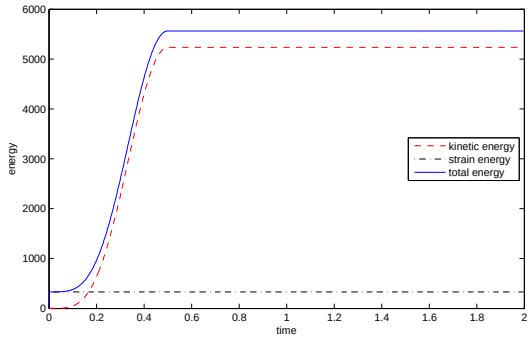

Figure 6: Energy versus time

5.2 Impact

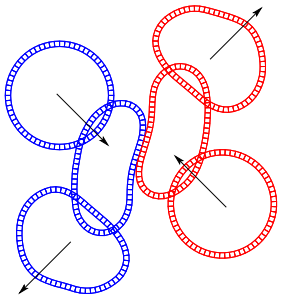

Figure 7: Snapshots of the motion

The present numerical example deals with the impact of two elastic rings. Similar examples have been previously considered by Wriggers et al. [17] and Laursen & Love [10]. This example is especially well-suited to check the algorithmic conservation properties.
64 isoparametric displacement-based bi-linear finite elements have been used to discretize each initially circular ring. The material behavior of both rings is assumed to be governed by the St. Venant-Kirchhoff material model with Young's modulus $E = 100$ and Poisson's ratio $\nu = 0.1$. The mass density of both rings is $\varrho_R = 0.001$. The two rings move towards each other with an initial velocity of $v_0 = 10$. In the simulations documented below a time-step of $\Delta t = 0.01$ has been used. To illustrate the simulated motion snapshots of the two rings at successive points in time are depicted in Fig. 7. After the initial free-flight phase contact takes place within the time interval of approximately $[6, 16]$.

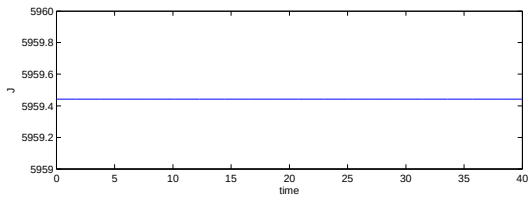

Figure 8: Total angular momentum versus time

Since no external forces/torques act on the present two-body system the total linear momentum as well as the total angular momentum are conserved quantities. These momenta are indeed conserved by the proposed algorithm, see Fig. 8. Furthermore, algorithmic conservation of the total energy follows from Fig. 9.

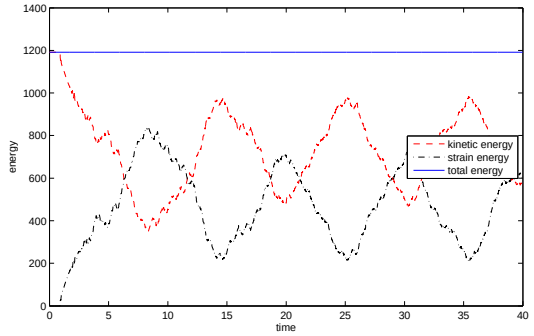

Figure 9: Energy versus time

6 Conclusions

The main new contribution of the present work lies in the design of the algorithmic contact forces within the framework of the Mortar contact element. In particular, the newly-proposed parametrization of the Mortar contact constraints in terms of appropriate invariants along with the use of the notion of a discrete gradient are the main features which facilitate the design of an energy-momentum scheme. In the developments presented herein we have tacitly assumed that active nodes of contact have been properly detected.

References

[1] In P.G. Ciarlet and J.L. Lions, editors, *Handbook of Numerical Analysis*.

[2] S.S. Antman. *Nonlinear Problems of Elasticity*. Springer-Verlag, 2005.

[3] F. Armero and E. Petöcz. Formulation and analysis of conserving algorithms for frictionless dynamic contact/impact problems. *Comput. Methods Appl. Mech. Engrg.*, 158:269–300, 1998.

[4] T. Belytschko, W.J.T. Daniel, and G. Ventura. A monolithic smoothing-gap algorithm for contact-impact based on the signed distance function. *Int. J. Numer. Methods Engng.*, 55:101–125, 2002.

[5] P. Betsch and P. Steinmann. Conserving properties of a time FE method - Part II: Time-stepping schemes for non-linear elastodynamics. *Int. J. Numer. Methods Engng.*, 50:1931–1955, 2001.

[6] P. Betsch and P. Steinmann. Conservation properties of a time FE method. Part III: Mechanical systems with holonomic constraints. *Int. J. Numer. Methods Engng.*, 53:2271–2304, 2002.

[7] C.W. Gear, G.K. Gupta, and B.J. Leimkuhler. Automatic integration of the Euler-Lagrange equations with constraints. *J. Comp. Appl. Math.*, 12:77–90, 1985.

[8] O. Gonzalez. Time integration and discrete Hamiltonian systems. *J. Nonlinear Sci.*, 6:449–467, 1996.

[9] O. Gonzalez. Mechanical systems subject to holonomic constraints: Differential - algebraic formulations and conservative integration. *Physica D*, 132:165–174, 1999.

[10] T.A. Laursen. *Computational Contact and Impact Mechanics*. Springer, 2002.

[11] T.A. Laursen and V. Chawla. Design of energy conserving algorithms for frictionless dynamic contact problems. *Int. J. Numer. Methods Engng.*, 40:863–886, 1997.

[12] T.A. Laursen and G.R. Love. Improved implicit integrators for transient impact problems – geometric admissibility within the conserving framework. *Int. J. Numer. Methods Engng.*, 53:245–274, 2002.

[13] J.C. Simo and N. Tarnow. The discrete energy-momentum method. Conserving algorithms for nonlinear elastodynamics. *ZAMP*, 43, 1992.

[14] J.C. Simo, P. Wriggers, and R.L. Taylor. A perturbed Lagrangian formulation for the finite element solution of contact problems. *Comput. Methods Appl. Mech. Engrg*, 50:163–180, 1985.

[15] C. Truesdell and W. Noll. *The Non-Linear Field Theories of Mechanics*. Springer, 2004.

[16] P. Wriggers. *Computational contact mechanics*. John Wiley & Sons Ltd, 2002.

[17] P. Wriggers, T.V. Van, and E. Stein. Finite element formulations of large deformation impact-contact problems with friction. *Computers and Structures*, 37:319–331, 1990.